



PCCP

**Factors Contributing to Halogen Bond Strength and Stretch
or Contraction of Internal Covalent Bond**

Journal:	<i>Physical Chemistry Chemical Physics</i>
Manuscript ID	CP-ART-11-2022-005598.R1
Article Type:	Paper
Date Submitted by the Author:	05-Jan-2023
Complete List of Authors:	Michalczyk, Mariusz; Wrocław University of Science and Technology Kizior, Beata; Wrocław University of Science and Technology Zierkiewicz, Wiktor; Wrocław University of Science and Technology, Chemistry Scheiner, Steve; Utah State University, Department of Chemistry and Biochemistry

SCHOLARONE™
Manuscripts

Factors Contributing to Halogen Bond Strength and Stretch or Contraction of Internal Covalent Bond

Mariusz Michalczyk*,¹ Beata Kizior,¹ Wiktor Zierkiewicz,¹ and Steve Scheiner^{2*}

¹Faculty of Chemistry, Wrocław University of Science and Technology, Wybrzeże Wyspiańskiego 27, 50-370 Wrocław, Poland

²Department of Chemistry and Biochemistry, Utah State University Logan, Utah 84322-0300, United States

Abstract

The halogen bond formed by a series of Lewis acids TF_3X ($\text{T}=\text{C}, \text{Si}, \text{Ge}, \text{Sn}, \text{Pb}$; $\text{X}=\text{Cl}, \text{Br}, \text{I}$) with NH_3 are studied by quantum chemical calculations. The interaction energy is closely mimicked by the depth of the σ -hole on the X atom as well as the full electrostatic energy. There is a first trend by which the hole is deepened if the T atom to which X is attached becomes more electron-withdrawing: $\text{C} > \text{Si} > \text{Ge} > \text{Sn} > \text{Pb}$. On the other hand, larger more polarizable T atoms are better able to transmit the electron-withdrawing power of the F substituents. The combination of these two opposing factors leaves PbF_3X forming the strongest XBs, followed by CF_3X , with SiF_3X engaging in the weakest bonds. The charge transfer from the NH_3 lone pair into the $\sigma^*(\text{TX})$ antibonding orbital tends to elongate the covalent TX bond, and this force is largest for the heavier X and T atoms. On the other hand, the contraction of this bond deepens the σ -hole at the X atom, which would enhance both the electrostatic component and the full interaction energy. This bond-shortening effect is greatest for the lighter X atoms. The combination of these two opposing forces leaves the T-X bond contracting for $\text{X}=\text{Cl}$ and Br , but lengthening for I .

Keywords: molecular electrostatic potential; σ -hole; charge transfer; energy decomposition

*Correspondence to: mariusz.michalczyk@pwr.edu.pl, steve.scheiner@usu.edu

INTRODUCTION

As arguably the most important of all intermolecular interactions, the H-bond (HB) has deservedly received an enormous amount of attention over the century since its existence was established¹⁻⁶. The factors that contribute to its strength have been elucidated, as well as secondary issues such as the circumstances which propel the bridging proton to transfer from one subunit to the other⁷⁻¹⁴. An enormous body of work has developed the ability to estimate the strength of a given HB based upon spectroscopic data such as the downfield shift of the NMR signal of the central proton^{15, 16}. Another trademark of a $AH\cdots B$ H-bond is the bathochromic shift of the A-H stretching frequency, coupled with the intensification of this band in the IR spectrum¹⁷⁻²⁰. Detailed scrutiny has shown that this red shift is typically accompanied by a small elongation of this A-H bond.

One of the more intriguing developments in the H-bond field was the recent discovery that a number of HBs ignore this rule, and shift their AH stretching frequency to the blue²¹⁻³¹. In these cases, the bond length also changes in the opposite direction, contracting instead of elongating. After some initial thought that perhaps this contrary behavior disqualified these interactions as true H-bonds, it was soon agreed that they are indeed H-bonds in all respects, despite their unexpected spectral behavior. There have been a number of hypotheses advanced as to how to account for these unusual characteristics³²⁻⁵¹. The common theme in these varying ideas is that there are two sets of forces acting on the length of the A-H covalent bond in all cases, some pushing toward elongation while contraction is favored by others. The end result is simply due to the final balance between these two forces.

The halogen bond (XB)⁵²⁻⁵⁷ is one of a family of noncovalent bonds, including also chalcogen, pnictogen, and tetrel bonds⁵⁸⁻⁶⁵, in which the bridging proton of the HB is replaced by any of a large group of other elements. Because most of the halogen atoms are more electronegative than H, one cannot assign an overall positive charge to X as one can for H. Nonetheless, there is a high degree of anisotropy of electron density around X, which leads in turn to a positive region of the electrostatic potential that is focused along the extension of the A-X bond. This so-called σ -hole can attract a nucleophile in much the same way as can a proton with its partial positive charge. Also like the H-bond, there is a certain amount of charge that is transferred from the lone pair of the nucleophile into the $\sigma^*(AX)$ antibonding orbital of the $AX\cdots B$ halogen bond, accounting for some of the stability of this interaction.

Given the high degree of similarity between the nature of the HB and XB, it is natural to expect a parallel red shift of the AX stretching frequency, coupled with an elongation of the AX bond. And although the body of IR data for XBs is admittedly more meager than that for HBs, there does seem to be a trend in that direction. On the other hand, there have also been some observations of shifts in the opposite direction. As one example, the CI frequency⁶⁶ of iodomethane shifts toward the blue when coupled with ethanol. Contractions of the R-Cl bond occur when R= NO_2 , but elongations occur for other R groups⁶⁷. Red shifts characterize XBs to XCN, XCCH and XCCCN, but the changes are in the opposite direction for XCF_3 , XCF_2H and $XCFH_2$ ⁶⁸. Various FX units

all shift to the red ^{69, 70}, regardless of base. The CX bond is contracted, and its stretching frequency shifts to the blue ⁷¹ for a series of anesthetics engaged in CX··O XBs.

At this point, then, the reports are quite scattered in terms of development of a scheme to predict which systems behave in one manner or the other. Why do some systems undergo a bond elongation while contractions are seen in others? What is needed is a systematic study to identify the forces that control the direction of shift, so as to better predict how a given halogen-bonded system will behave. Such an understanding will enable a proper interpretation of spectra with regard to the presence and strength of any halogen bonds that might occur.

The current work addresses this question by applying high-level quantum chemical calculations to a series of fifteen different TF₃X molecules in which X represents each of the three halogen atoms Cl, Br, and I. Five different tetrel atoms C, Si, Ge, Sn, and Pb were included, covering a wide range of size, electronegativity, and polarizability. NH₃ was chosen as the universal nucleophile with which each Lewis acid partners in a halogen bond. Its moderate basicity is ideal for this study, and its small size largely precludes the complications that might arise from secondary interactions.

COMPUTATIONAL DETAILS

The Gaussian 16 ⁷² suite of programs was employed for quantum chemical calculations. Density functional theory (DFT) employed the M06-2X functional ⁷³, in the context of the aug-cc-pVTZ basis set which includes both polarization and diffuse functions added to a triple- ζ foundation. The aug-cc-pVTZ-PP pseudopotential ⁷⁴ was applied to Sn, Pb and I as it takes into account certain relativistic effects. The geometries of monomers and complexes were optimized with no symmetry constraints, and were verified as true minima by normal mode analysis. Each interaction energy E_{int} is defined as the difference between the energy of the dyad and the sum of the energies of the two monomers in the geometry they adopt within the dimer. Basis set superposition error was then removed from E_{int} by the standard counterpoise protocol ⁷⁵. Decomposition of the interaction energies was carried out at the M06-2XD/ZORA/TZ2P level of theory through the ADF-EDA protocol according to the Morokuma-Ziegler scheme embedded in ADF software ⁷⁶⁻⁷⁸ (the dispersion keyword was used). The M062XD functional was applied to this scheme along with a slight variation in basis set in order to fully capture dispersive contributions. The NBO method ^{79, 80} as incorporated in Gaussian, was applied to quantify interorbital charge transfers and their energetic manifestation. The MultiWFN program ⁸¹ located the maxima of the molecular electrostatic potential (MEP) on the $\rho=0.001$ au isodensity surface of each monomer.

RESULTS

Fifteen F₃TX Lewis acid molecules were constructed with T=C, Si, Ge, Sn, and Pb, and X=Cl, Br, or I. Each was then allowed to form a dimer with the base NH₃ which was held together by a X··N halogen bond. Examples of three such dyads are illustrated in Fig 1.

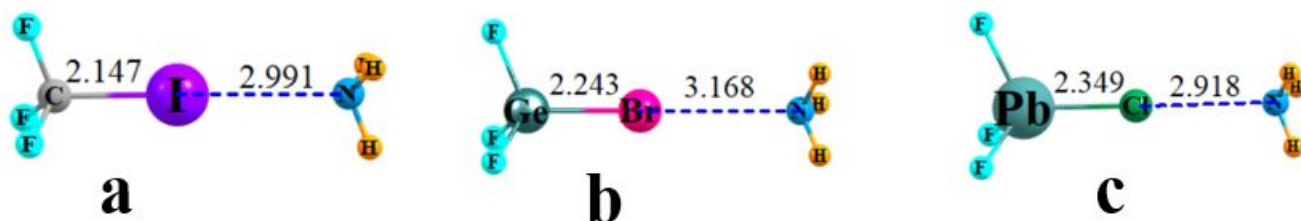


Fig 1. Geometries of three sample halogen-bonded complexes. Distances in Å.

Properties of Halogen Bonds

The first column of data in Table 1 lists the values of the maximum on the 0.001 au isodensity surface along the extension of each T-X bond, the so-called σ -hole depth on X, as V_{\max} . For any particular T atom, the hole deepens as the X atom grows in size $\text{Cl} < \text{Br} < \text{I}$. The dependence upon the identity of the tetrel atom is a bit more nuanced. The depth of the hole is largest at the two extremes, C and Pb, with the latter generally having the largest V_{\max} . The σ -hole is smallest for Si, leading to an overall pattern of $\text{Pb} > \text{C} > \text{Ge} \sim \text{Sn} > \text{Si}$. The total dipole moment of the Lewis acid monomer follows a clearer order in which it grows along with the size of both the T and X atoms. The next column of Table 1 displays the interaction energy that occurs when each Lewis acid complexes with NH_3 . This quantity spans a wide range from 1.3 to 9.9 kcal/mol. These energies follow along with the pattern noted above for V_{\max} for the most part: E_{int} grows quickly as X becomes heavier. The interaction energies are largest for Pb, followed by C, with Si associated with the weakest binding. Indeed, there is a close relationship between E_{int} and V_{\max} , with a correlation coefficient $R^2=0.95$.

The intermolecular XB distances in the next column are all in the 3 Å range, between 2.8 and 3.3 Å. Despite the larger radii of the heavier X atoms, $R(\text{X}\cdots\text{N})$ does not elongate; rather, the strengthening XB tends to contract this distance even if only slightly. The XB length is shortest for the Pb complexes, attributed to their greatest strength, with the C distances in the first three rows a bit longer, followed then by the other complexes with longer XB lengths. Perhaps a better yardstick as to the XB length factors out the intrinsic atomic radii which differs from one atom to the next.

Table 1. Properties of optimized monomers F_3TX , and complexes with NH_3

Monomer	V_{\max} , kcal/mol	μ_{mon} , D	$-E_{\text{int}}$, kcal/mol	$R(\text{X}\cdots\text{N})$, Å	R_{N}	$r(\text{TX})_{\text{mon}}$, Å	$r(\text{TX})_{\text{dim}}$, Å
$\text{F}_3\text{C-Cl}$	21.37	0.473	2.52	3.030	0.84	1.757	1.751
$\text{F}_3\text{C-Br}$	25.13	0.578	3.74	3.006	0.83	1.927	1.924

F ₃ C-I	32.16	1.020	6.09	2.991	0.79	2.143	2.147
F ₃ Si-Cl	14.19	0.715	1.28	3.340	0.83	2.003	1.998
F ₃ Si-Br	18.66	0.902	2.04	3.264	0.81	2.167	2.162
F ₃ Si-I	24.58	1.301	3.36	3.273	0.77	2.382	2.383
F ₃ Ge-Cl	17.70	1.281	1.83	3.183	0.77	2.094	2.089
F ₃ Ge-Br	23.85	1.740	2.94	3.168	0.76	2.245	2.243
F ₃ Ge-I	31.85	2.489	4.82	3.151	0.73	2.450	2.456
F ₃ Sn-Cl	16.53	1.616	1.84	3.168	0.75	2.273	2.270
F ₃ Sn-Br	23.83	2.263	3.15	3.142	0.73	2.417	2.416
F ₃ Sn-I	33.20	3.290	5.30	3.108	0.70	2.611	2.620
F ₃ Pb-Cl	21.88	2.365	3.42	2.918	0.66	2.347	2.349
F ₃ Pb-Br	31.10	3.310	5.70	2.869	0.64	2.483	2.493
F ₃ Pb-I	43.59	4.833	9.88	2.777	0.60	2.666	2.703

The normalized distance R_N in Table 1 divides $R(X\cdots N)$ by the sum of vdW radii of the two atoms involved⁸². The small ratios less than 0.7 for the Pb complexes reflect the strength of these bonds. It is interesting that R_N is largest for the C dyads despite their strength, second only to Pb. But in any case, all the normalized distances are comfortably smaller than unity, consistent with the presence of a moderately strong XB. The last two columns of Table 1 contain the internal T-X distances within the optimized monomers and dimers. It is evident that there is contraction occurring in some and elongation in others upon complexation.

Table 2 reports the results of decomposition of the interaction energies of the various complexes. It is immediately clear that the electrostatic term outweighs the orbital interaction quantity. E_{ES} accounts for between 60 and 66% of the total attraction, leaving the remainder to E_{OI} and E_{Disp} . The importance of E_{ES} is also reflected by its tight relationship with the full interaction energy, with correlation coefficient 0.99. A large portion, but certainly not all, of the electrostatic component is connected with the interaction between the X σ -hole and the negative region of the NH₃ unit. Likewise, a major portion of the orbital interaction term arises from the transfer of charge from the NH₃ lone pair into the $\sigma^*(TX)$ antibonding orbital, as discussed in more detail below. The correlations of E_{OI} and E_{Disp} with E_{int} are not as good, with correlation coefficients of 0.93 and 0.78, respectively.

Table 2. EDA/M06-2XD/ZORA/TZ2P decomposition of the interaction energy of complexes into Pauli repulsion (E_{Pauli}), electrostatic (E_{ES}), orbital interaction (E_{oi}) and dispersion (E_{disp}) components. All energies in kcal/mol.

Dimer	E_{Pauli}	E_{ES}	%	E_{OI}	%	E_{disp}	%	E_{int}
-------	-------------	----------	---	----------	---	------------	---	-----------

F ₃ C-Cl⋯NH ₃	3.95	-4.82	66	-1.70	23	-0.78	11	-3.35
F ₃ C-Br⋯NH ₃	6.21	-7.33	66	-2.90	26	-0.95	8	-4.97
F ₃ C-I⋯NH ₃	11.17	-12.16	66	-4.97	27	-1.17	6	-7.14
F ₃ Si-Cl⋯NH ₃	1.43	-2.08	62	-0.61	18	-0.65	19	-1.91
F ₃ Si-Br⋯NH ₃	2.80	-3.80	64	-1.23	21	-0.93	16	-3.16
F ₃ Si-I⋯NH ₃	4.75	-6.05	66	-1.95	21	-1.16	13	-4.41
F ₃ Ge-Cl⋯NH ₃	2.53	-3.42	65	-1.10	21	-0.76	14	-2.75
F ₃ Ge-Br⋯NH ₃	3.82	-5.29	65	-1.90	23	-0.97	12	-4.34
F ₃ Ge-I⋯NH ₃	6.97	-8.70	66	-3.25	25	-1.17	9	-6.15
F ₃ Sn-Cl⋯NH ₃	2.71	-3.29	62	-1.23	23	-0.79	15	-2.60
F ₃ Sn-Br⋯NH ₃	4.32	-5.53	63	-2.21	25	-0.99	11	-4.41
F ₃ Sn-I⋯NH ₃	8.35	-9.66	66	-3.82	26	-1.18	8	-6.31
F ₃ Pb-Cl⋯NH ₃	6.49	-6.53	60	-3.48	32	-0.86	8	-4.39
F ₃ Pb-Br⋯NH ₃	10.97	-11.11	61	-6.11	33	-1.05	6	-7.30
F ₃ Pb-I⋯NH ₃	24.27	-21.93	62	-12.18	34	-1.41	4	-11.25

Explanation of Trends

Some of the trends contained within Table 1 are entirely consistent with prior calculations and chemical principles. For example, the σ -hole deepens as the X atom becomes larger, in line with its growing polarizability and electropositivity. This pattern is mimicked by the full electrostatic component of the interaction, as well as the total interaction energy itself.

On the other hand, the dependence of the various aspects of the XB upon the tetrel atom to which the halogen atom is attached is a bit more subtle. If one were to contemplate the source of the σ -hole on the X atom, it would be logical to expect it to be deepest for the most electronegative T atom which ought to best draw density away from X. The actual values of tetrel electronegativities vary a bit from one scale to another but there is a general trend for diminishing electronegativity with larger atom. V_{\max} changes in the direction opposite to this expectation, rising as: Si < Ge < Sn < Pb. The notable exception to this pattern is C for which V_{\max} is suitably large, second only to Pb. This order of σ -hole depth persists in the full electrostatic component, as well as E_{int} . The dipole moments of the monomers also increase with larger T atom, but without the anomaly for F₃CX for which μ is smallest of all the monomers.

This pattern may be reflective of two opposing forces. On one hand, the more electronegative tetrel atoms near the top of the periodic table like C will exert a stronger pull on the electron density of the X atom, tending to deepen its σ -hole. On the other hand, the more polarizable T atoms

toward the bottom of the table can better facilitate the electron-withdrawing power of the F atoms to propagate through to the X atom, drawing density away from X and deepening the σ -hole.

In order to test this hypothesis, the series of TH_3Br and TH_3I monomers were examined in which the F atoms have been entirely removed, negating the second issue above. The solid curves in Fig 2 graphically illustrate the σ -hole depths for the perfluorosubstituted molecules extracted from Table 1. The behavior of V_{max} for their non-fluorinated analogues is displayed as the broken curves. Without the F atoms to draw density away from X, these σ -holes are of course shallower than those for F_3TX . But most important is the monotonic decrease of V_{max} as the T atom grows larger. This pattern is entirely consistent with the reduced ability of the heavier T atoms to withdraw density from X. When the F atoms are added, however, this trend is countered by the better ability of F to draw density away from X as the T atom grows larger and more polarizable. The combined result of these two opposing factors leads to the minimum observed in the solid curves for $\text{T}=\text{Si}$.

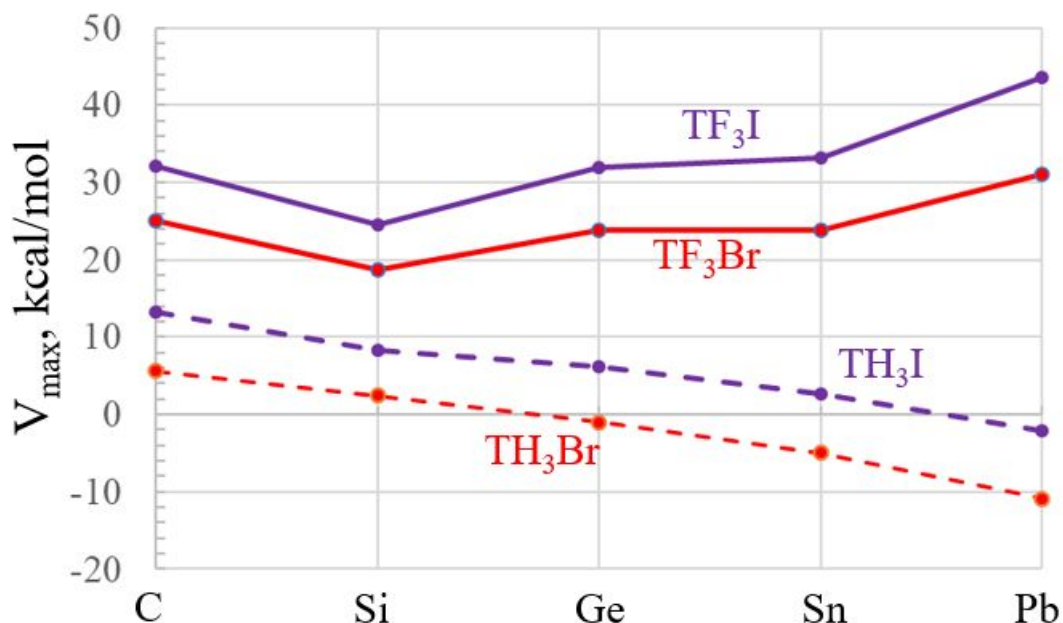


Fig 2. Variation of σ -hole depth on X atom for indicated monomers, for various tetrel T atoms.

Internal Perturbations

The effect of the formation of each XB upon the internal covalent T-X bond length is highlighted in the first column of data of Table 3. There are certain trends which are clear from this data. The bond tends to contract for the lighter X atom, and to elongate as X grows larger. Taking the Ge dyads as an example, Δr is equal to -0.005 \AA for $\text{X}=\text{Cl}$, -0.002 \AA for Br, and then undergoes a lengthening of 0.006 \AA for F_3GeI . With regard to the nature of the T atom, the heavier atoms are associated with less of a contraction, and/or more of an elongation. This trend is

particularly evident for Pb, for which the Pb-X bond elongates for all three X atoms, growing quickly from only 0.002 Å for Cl, up to 0.037 Å for I.

Table 3. Change in internal $r(\text{TX})$ bond length and TX stretching frequency caused by complexation, $\text{N}_{\text{lp}} \rightarrow \sigma^*(\text{TX})$ charge transfer, and percentage changes caused in properties resulting from contracting $r(\text{TX})$ by 0.1 Å.

Lewis acid	$\Delta r(\text{T-X}), \text{Å}$	$E(2), \text{kcal/mol}$	$\Delta V_{\text{max}}, \%$	$\Delta \mu, \%$	$\Delta E_{\text{ES}}, \%$	$\Delta \nu(\text{T-X}), \text{cm}^{-1}$
$\text{F}_3\text{C-Cl}$	-0.006	2.70	11.3	63.6	4.3	-0.4
$\text{F}_3\text{C-Br}$	-0.003	5.11	6.0	39.8	1.2	-4.8
$\text{F}_3\text{C-I}$	0.004	8.92	1.6	12.2	-0.5	-8.8
$\text{F}_3\text{Si-Cl}$	-0.005	0.72	16.9	54.0	11.4	3.0
$\text{F}_3\text{Si-Br}$	-0.005	1.67	8.6	37.7	4.1	1.7
$\text{F}_3\text{Si-I}$	0.001	2.96	2.9	20.4	0.5	0.6
$\text{F}_3\text{Ge-Cl}$	-0.005	1.44	13.0	28.5	6.8	4.7
$\text{F}_3\text{Ge-Br}$	-0.002	2.72	6.5	18.3	2.8	1.9
$\text{F}_3\text{Ge-I}$	0.006	4.95	2.0	9.5	0.2	1.6
$\text{F}_3\text{Sn-Cl}$	-0.003	1.74	13.1	22.2	6.8	2.7
$\text{F}_3\text{Sn-Br}$	-0.001	3.32	6.7	14.0	2.7	1.0
$\text{F}_3\text{Sn-I}$	0.009	6.12	2.3	7.3	0.4	-0.4
$\text{F}_3\text{Pb-Cl}$	0.002	4.38	10.0	14.5	3.5	-8.4
$\text{F}_3\text{Pb-Br}$	0.010	8.29	5.2	8.7	1.3	-11.8
$\text{F}_3\text{Pb-I}$	0.037	17.13	1.7	3.7	0.0	-12.6

There are two primary forces acting upon this internal bond length. On the one hand, one distinguishing feature of a halogen bond is a certain amount of charge transfer from the N lone pair into the $\sigma^*(\text{TX})$ orbital. The accumulation of density into this antibonding orbital would tend to elongate this bond, which in fact leads to the stretches that are commonly observed in the majority of XBs. The energetic manifestation of this charge transfer is listed in the next column of Table 3 as the NBO value of $E(2)$. These quantities are reflective of the overall bond strengths in the sense that $E(2)$ grows along with the size of X. It also enlarges with a heavier T atom, with the exception of C which is second only to Pb. Indeed, $E(2)$ bears a strong resemblance to E_{int} , with a correlation coefficient between them of 0.96. And in fact, the pattern for $E(2)$ closely mirrors the overall orbital interaction term E_{OI} listed in Table 1, with a correlation coefficient between these two quantities of 0.98.

The second important factor originates with the electronic distribution within the Lewis acid molecule and how it is affected by geometry changes. If a contraction of the T-X bond were to deepen the σ -hole on the X atom, the attendant enhancement of the attraction with the negative region of the base would stabilize the system. This promise of a lower energy would counter the charge transfer tendency pushing toward a longer $r(\text{TX})$. The ΔV_{max} column of Table 3 reports the percentage change in the σ -hole depth that arises from a 0.1 Å contraction of the TX bond within each isolated F_3TX monomer. (This quantity was calculated as the difference between a 0.05 Å reduction and a 0.05 Å stretch.) In all cases, the σ -hole is deepened by the contraction, with positive values of ΔV_{max} . This intensification is greatest for the smaller X atoms, above 10% for Cl, and less than 3% for I. So the σ -hole deepening seen here ought to push each internal TX bond toward a contraction, particularly for the lighter X atoms, as such a shortening would enhance the σ -hole.

Another perspective on the electrostatic interaction with the base can be gleaned from the dipole moment of the Lewis acid molecule. This property is aligned along the T-X axis, with its positive end toward X. Like V_{max} , the dipole moment in the next column of Table 3 is also raised by the 0.1 Å contraction of $r(\text{TX})$. Also in common with σ -hole depth, this increase is most appreciable for the lighter X atoms, but still present even for I. So both V_{max} and μ would push the system toward a shorter $r(\text{TX})$.

One can test the presumption that a deeper σ -hole or increased μ would raise the electrostatic attraction between the two molecules by calculating the electrostatic component of the interaction energy via an energy decomposition scheme, as reported earlier in Table 2. This attractive element is indeed raised when the internal $r(\text{TX})$ bond is shortened, as witness the positive values in the penultimate column of Table 3. Of particular relevance, the trends in ES largely mirror those in both ΔV_{max} and $\Delta\mu$. The rise in the E_{ES} component is largest for the lighter of the X atoms, nearly disappearing for I.

In summary, the trends in Δr can be explained by the combination of two simple effects. The charge transfer into the antibonding orbital pushes toward elongation, and this trend is greatest for the larger X atoms. The electrostatic forces on the other hand, as exemplified by σ -hole depth, dipole moment, or ES itself, tend toward a shorter r , and this effect is strongest for the smaller X atoms.

These opposing trends can be visualized by plotting each of the relevant properties against the bond length change that occurs upon complexation. The left side of Fig 3, with its negative values of Δr , corresponds to bond contractions, switching to stretches as one moves to the right. The propensity of E(2) to push the system toward longer r is clearly evident by the upward slope of the red curve. That is, increased charge transfer is consistent with bond elongation. The green curve refers to the change in σ -hole depth upon 0.1 Å contraction of r within the monomer. The largest rises in V_{max} are clustered on the left side of Fig 2 along with the bond contractions which they cause. Attenuation of ΔV_{max} toward the right side allows the bond-lengthening effects of E(2) to predominate, and Δr becomes positive. The parallel behavior of ES reduction, indicated by the black curve, shows that the behavior of the σ -hole is mirrored by the full electrostatic component.

In sum, the large values of $E(2)$ on the right, combined with the smaller magnitude of the electrostatic elements, result in bond stretching. The bond contraction toward the left is made possible by the domination of the growing influence of electrostatic effects, in concert with the attenuation of the lengthening effects of charge transfer.

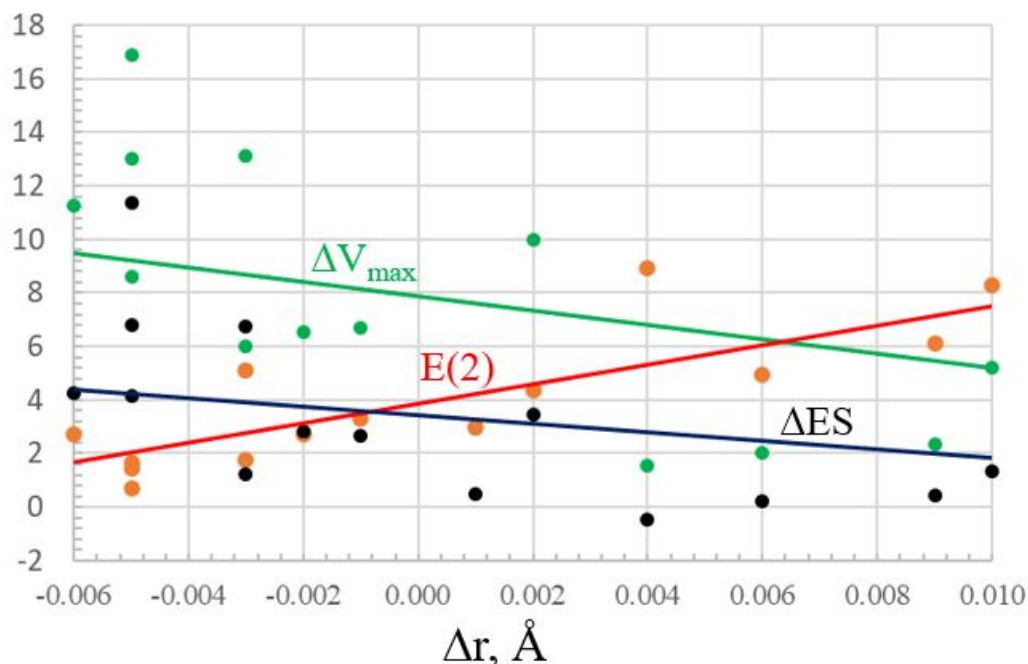


Fig 3. Increase in σ -hole depth ΔV_{\max} of Lewis acid that accompanies 0.1 \AA shortening of internal $r(\text{TX})$ bond, as percentage of value in optimized monomer (green). ΔES (black) refers to the percentage rise in the electrostatic component of the interaction energy within the complex with NH_3 that arises upon 0.1 \AA reduction of $r(\text{TX})$. Also displayed is the NBO $\text{N}_{\text{lp}} \rightarrow \sigma^*(\text{TX})$ charge transfer energy $E(2)$ within the complex (red), in kcal/mol. All quantities are plotted against the change in the T-X bond length that occurs upon complexation with NH_3 . $\text{F}_3\text{Pb-I}$ system has not been included explicitly as its values lie far to the right.

As a second manifestation of this confluence of opposing forces, the very shallow σ -holes of the nonfluorinated TH_3X monomers reduce their ability to engage in a XB with NH_3 . Indeed, it is only several of the TH_3I units which can engage in such a bond with NH_3 , and only for the lighter C, Si, and Ge tetrel atoms on the left side of Fig 2, with their higher values of V_{\max} . The essential features of these complexes are reported in Table 4 where it may be seen that the XB energy is largest for H_3CI and declines as T grows larger. This pattern is mimicked by $E(2)$ although there is only a small difference between Si and Ge. The contraction of the CI distance within the H_3CI monomer results in a very small reduction in the I σ -hole, whereas V_{\max} is increased by this $r(\text{TI})$ contraction for both Si and Ge. The large charge transfer into the $\sigma^*(\text{CI})$ antibonding orbital causes the CI bond to elongate, as evident in the last column of Table 4, which is actually reinforced by

the small intensification of the σ -hole arising from this stretch. For the H_3SiI and H_3GeI systems, in contrast, the contraction of the $r(\text{TI})$ bond is favored by its attendant deepening of the I σ -hole. This contracting effect cannot be effectively countered by any lengthening force that arises from the smaller values of $E(2)$. As a result, $\Delta r(\text{T-X})$ is negative in the last two rows of Table 4.

Table 4. Interaction energy, $N_{\text{lp}} \rightarrow \sigma^*(\text{TX})$ charge transfer, percentage change caused in σ -hole depth resulting from contracting $r(\text{TX})$ by 0.1 \AA , and change in internal $r(\text{TX})$ bond length caused by complexation with NH_3 .

Lewis acid	$-E_{\text{int}}$, kcal/mol	$E(2)$, kcal/mol	ΔV_{max} , %	$\Delta r(\text{T-X})$, \AA
$\text{H}_3\text{C-I}$	2.71	4.58	-2.3	0.0044
$\text{H}_3\text{Si-I}$	1.41	1.91	+12.9	-0.0024
$\text{H}_3\text{Ge-I}$	1.28	2.02	+18.5	-0.0035

As a final issue, it is usually thought that the stretch/contraction of the T-X bond ought to correspond respectively to a red or blue shift of its vibrational frequency. This idea represents an extension of the association usually drawn for the covalent AH bond in a H-bonded $\text{AH}\cdots\text{B}$ complex. The correspondence is not quite as simple as that since the T-X stretching motion is not a pure one. This normal mode is intimately connected with the puckering of the TF_3 group to which it the X is connected, a symmetric bend of sorts. Further, there are elements of the T-X stretching motion contained in other normal modes to varying degrees. In any case, the change in the frequency of this mode that arises upon XB formation with NH_3 is displayed in the final column of Table 3. It is immediately apparent that a contraction of the T-X bond does not necessarily lead to an increase in ν . F_3CBr is a case in point in that the C-Br bond contracts by 0.003 \AA but the frequency nonetheless shifts to the red by 4.8 cm^{-1} .

But it is equally clear that there is a connection between the degree of contraction or stretch and the change in the frequency. For any given T atom, the change from Cl to Br to I causes both a trend toward a bond lengthening and a “redder” shift, whether more negative or less positive. And those complexes containing Pb, all of which display a stretch of the Pb-X bond, are all associated with red shifts. The overall correlation coefficient between Δr and $\Delta \nu$ is only mediocre, equal to 0.47, which is perhaps understandable in light of the high degree of contamination of the T-X stretching motion within this normal mode.

DISCUSSION

There have been several prior studies of XBs involving F_3TX such as F_3CCl with NH_3 ⁸³. A recent systematic examination⁸⁴ echoed the findings here that the weakest XB of F_3TX occurs for T=Si , and that the T-X bond contracts for X=Cl and Br but stretches when X=I . Another study⁸⁵ considered $\text{CF}_3\text{X}\cdots\text{NH}_3$ complexes with an eye toward the origin of XB directionality. $\text{CF}_3\text{X}\cdots\text{N}$ halogen bonds had been experimentally identified in solution⁸⁶, in this case with trimethylamine base. The computed data affirm the finding here that the lighter X atoms tends toward bond

shortening, while elongation is characteristic of the heavier halogens. Bramlett and Matzger⁸⁷ measured red shifts of the C-I stretching frequency of iodinated phenyl rings of roughly 4-7 cm^{-1} in CH_2Cl_2 solution when involved in I \cdots N XBs, consistent with the T-I stretches computed here.

There are other examples in the literature wherein formation of a halogen bond induces a contraction of the covalent bond to the X atom. Mo *et al.*⁸⁸ considered the contributions made by various factors to the red or blue shifts of XBs, albeit different complexes than those discussed above, with X bonded to either another X atom or a NO_2 group. The internal bond length elongates in the former case, but contracts in the latter. Like the systems described here, the authors observed a lessening of the bond contraction as one progresses from Cl to Br to I. Calculations were carried out of these systems in order to test the ideas proposed here. It was found that contraction of the N-X bond in $\text{O}_2\text{N-X}$ monomers deepens the X σ -hole by 17, 11, and 6% respectively for X=Cl, Br, and I. So again, one sees the same pattern as for the TF_3X monomers, wherein bond contraction is favored by electrostatic considerations, and this trend is greatest for the smaller X atoms. In further agreement with this perspective, Torii⁸⁹ had earlier found the N-Cl bond of $\text{O}_2\text{N-Cl}$ contracted upon XB formation, along with a blue shift of its stretching frequency.

Other work further verifies these ideas. Very recent calculations⁵² had considered replacement of the F substituents of the CF_3X subunit by another electron-withdrawing group CN. Formation of a XB with NMe_3 does not contract the internal C-X bond of $\text{C}(\text{CN})_3\text{X}$, even for X=Cl and Br, yielding instead a stretch of several percent when complexed. Calculations in this laboratory of this series of molecules revealed that the 0.1 Å contraction of the C-X bond length has only a very minimal effect on the X σ -hole, deepening it by less than 5%. So the electrostatic effect is too small to counteract the bond lengthening arising from the accumulating density in the $\sigma^*(\text{CX})$ antibonding orbital. C-I stretches were recently noted for XBs formed by heptafluoro-2-iodopropane with I attached to a substituted alkane⁹⁰, similar to the elongations within the TF_3I units noted above.

Aliphatic CCl and CBr bonds are slightly contracted when engaged in $\text{CX}\cdots\text{O}$ XBs⁷¹ to CH_2O , confirming the same trends reported here. An earlier study had attached X to the C atom of the cyano group⁹¹ and the data confirm the strengthening of the XB as X grows larger. This work buttresses the conclusion drawn here that the degree of $r(\text{CX})$ stretching rises as X grows in size. Extended alkynyl and alkenyl chains were also attached to I atoms as well as substituted phenyl rings^{92,93}. The CI bond stretched in all the halogen bonded complexes with NH_3 , again consistent with the findings in the TF_3I Lewis acids examined here. C-I stretches were also noted for heptafluoro-2-iodopropane with I attached to a substituted alkane⁹⁰.

There has been further work which considered halogen atoms bound to atoms other than T such as N as in a halogenated succinimide⁹⁴ or directly to metal atoms⁹⁵. When bonded simply to a F atom, the FX series of Lewis acids elongate upon complexation with NH_3 , with a corresponding $\Delta\nu(\text{FX})$ stretching red shift⁷⁰ but the amount of this elongation is relatively uniform from one X to the next. Positively charged C-X donors have been considered within the context of halogenated imidazoliums⁹⁶ and continue the trend in neutral systems for the XB to intensify

with growing X size, in concert with a deepening σ -hole and rapidly growing E(2). All C-X distances are elongated by the XB, in the I > Br > Cl order.

Some of the issues discussed here are in line with earlier work. Wang and Hobza⁹⁷ agree that the charge transfer into the σ^* antibonding orbital is a major factor in any bond lengthening within a XB. The effects of electrostatics are attributed not to the σ -hole on the X atom, however, but to atomic charges of the atom to which the X is attached.

CONCLUSIONS

There are two principal factors that control the strength of the halogen bonds formed by the R_3TX molecule, both centering on the depth of the σ -hole on the X atom. On one hand, a more electronegative T atom such as the light C will draw density toward itself and deepen this hole. It is for this reason that CH_3I contains the deepest I σ -hole which weakens progressively as T grows larger. Consequently CH_3I engages in a stronger XB than do SiH_3I or GeH_3I , and the heavier Sn and Pb analogues are incapable of such a bond. However, when the R substituents on T are themselves electron-withdrawing, as F for example, a larger and more polarizable T will better enable these F atoms to extract density from X. The confluence of these two opposing forces leads to the mixed trend of σ -hole depth of the perfluorosubstituted TF_3X units: Pb > C > Sn > Ge > Si, which mimics the same trend in overall binding energy.

In the same vein, there are two competing issues that control whether the internal covalent T-X bond will contract or stretch as a result of halogen bond formation. Charge transfer from the lone pair of the base into the antibonding $\sigma^*(TX)$ orbital will weaken the bond and induce stretching. However, if the contraction of this bond within the monomer causes a deepening of the X σ -hole, coupled with increasing molecular dipole moment, then there will be an electrostatic force pushing toward a bond shortening. Regarding the first factor, the amount of charge transfer into the $\sigma^*(TX)$ orbital rises for the larger X atoms: Cl < Br < I, which would lead to a progressively greater tendency toward bond elongation. On the other hand, the TF_3X molecules all show a σ -hole deepening with T-X bond contraction, which is proportionately largest for the smaller X atoms: Cl > Br > I, so the lighter atoms would experience the strongest pull toward bond shortening. When these two opposing factors are combined, the net result is that most of the T-Cl bonds are contracted upon complexation, whereas T-I bonds are stretched, with mixed changes of small magnitude for T-Br. Due to the aforementioned Pb > C > Sn > Ge > Si pattern of σ -hole depth, and its resulting bond energy and charge transfer within the complex, there is a concomitant pattern that bond elongation increases (or bond contraction decreases) in this same order.

Despite contamination of the T-X stretching normal mode by other atomic motions, in particular the symmetric bending of the TF_3 group, there is a clear tendency for those systems in which the T-X bond contracts as a result of XB formation to shift the vibrational frequency toward the blue, and vice versa.

Author Contributions:

MM: Data curation, Formal Analysis, Investigation, Visualization, Writing - original draft;
BK: Formal Analysis, Investigation, Software, Visualization;
WZ: Data curation, Methodology, Supervision, Resources, Funding acquisition, Visualization;
SS: Conceptualization, Writing-Original and Final Draft, Funding acquisition, Visualization.

Funding

This research was funded by the Polish Ministry of Science and Higher Education for the Faculty of Chemistry of Wroclaw University of Science and Technology under Grant No. 8211104160/K14W03D10 and by the US National Science Foundation under Grant No. 1954310.

Acknowledgments

This work was financed in part by a statutory activity subsidy from the Polish Ministry of Science and Higher Education for the Faculty of Chemistry of Wroclaw University of Science and Technology and by the US National Science Foundation under Grant No. 1954310. A generous allotment of computer time from the Wroclaw Supercomputer and Networking Center is acknowledged.

Conflicts of Interest

The authors declare no conflict of interest.

REFERENCES

1. G. C. Pimentel and A. L. McClellan, *The Hydrogen Bond*, Freeman, San Francisco, 1960.
2. P. Schuster, G. Zundel and C. Sandorfy, *The Hydrogen Bond. Recent Developments in Theory and Experiments*, North-Holland Publishing Co., Amsterdam, 1976.
3. S. Cybulski and S. Scheiner, *J. Am. Chem. Soc.*, 1987, **109**, 4199-4206.
4. G. A. Jeffrey and W. Saenger, *Hydrogen Bonding in Biological Structures*, Springer-Verlag, Berlin, 1991.
5. S. Scheiner, *J. Indian Inst. Sci.*, 2020, **100**, 61-76.
6. S. Scheiner, D. A. Kleier and W. N. Lipscomb, *Proc. Nat. Acad. Sci., USA*, 1975, **72**, 2606-2610.
7. X. Pang, C. Jiang, W. Xie and W. Domcke, *Phys. Chem. Chem. Phys.*, 2019, **21**, 14073-14079.
8. K. Kamiya, M. Boero, M. Tateno, K. Shiraishi and A. Oshiyama, *J. Am. Chem. Soc.*, 2007, **129**, 9663-9673.
9. M. Cuma, S. Scheiner and T. Kar, *J. Mol. Struct. (Theochem)*, 1999, **467**, 37-49.
10. P. Chatterjee, A. K. Ghosh, M. Samanta and T. Chakraborty, *J. Phys. Chem. A*, 2018, **122**, 5563-5573.
11. M. V. Vener and S. Scheiner, *J. Phys. Chem.*, 1995, **99**, 642-649.
12. R. Neutze, E. Pebay-Peyroula, K. Edman, A. Royant, J. Navarro and E. M. Landau, *Biochim. Biophys. Acta - Biomemb.*, 2002, **1565**, 144-167.
13. K. Luth and S. Scheiner, *J. Phys. Chem.*, 1994, **98**, 3582-3587.
14. S. Scheiner and L. Wang, *J. Am. Chem. Soc.*, 1993, **115**, 1958-1963.
15. V. Dohnal and M. Tkadlecova, *J. Phys. Chem. B*, 2002, **106**, 12307-12310.

16. M. A. Massiah, C. Viragh, P. M. Reddy, I. M. Kovach, J. Johnson, T. L. Rosenberry and A. S. Mildvan, *Biochem.*, 2001, **40**, 5682-5690.
17. L. A. Rivera-Rivera, B. A. McElmurry, K. W. Scott, R. R. Lucchese and J. W. Bevan, *J. Phys. Chem. A*, 2013, **117**, 8477-8483.
18. M. Rozenberg, A. Loewenschuss and Y. Marcus, *Phys. Chem. Chem. Phys.*, 2000, **2**, 2699-2702.
19. P. R. Bangal and S. Chakravorti, *J. Phys. Chem. A*, 1999, **103**, 8585-8594.
20. M. H. Abraham, D. V. Prior, R. A. Schulz, J. J. Morris and P. J. Taylor, *Journal*, 1998, **94**, 879-885.
21. I. Bhattacharya, J. Sadhukhan, S. Biswas and T. Chakraborty, *J. Phys. Chem. A*, 2020, **124**, 7259-7270.
22. G. Karir and E. D. Jemmis, *J. Indian Inst. Sci.*, 2020, **100**, 127-133.
23. P. Ramasami and T. A. Ford, *Mol. Phys.*, 2018, **116**, 1722-1736.
24. R. Gopi, N. Ramanathan and K. Sundararajan, *Chem. Phys.*, 2016, **476**, 36-45.
25. R. Gopi, N. Ramanathan and K. Sundararajan, *J. Phys. Chem. A*, 2014, **118**, 5529-5539.
26. P. R. Shirhatti, D. K. Maity, S. Bhattacharyya and S. Wategaonkar, *ChemPhysChem.*, 2014, **15**, 109-117.
27. P. R. Shirhatti, D. K. Maity and S. Wategaonkar, *J. Phys. Chem. A*, 2013, **117**, 2307-2316.
28. W. Zierkiewicz, B. Czarnik-Matuszewicz and D. Michalska, *J. Phys. Chem. A*, 2011, **115**, 11362-11368.
29. B. Michielsen, J. J. J. Dom, B. J. van der Veken, S. Hesse, Z. Xue, M. A. Suhm and W. A. Herrebout, *Phys. Chem. Chem. Phys.*, 2010, **12**, 14034-14044.
30. A. A. Howard, G. S. Tschumper and N. I. Hammer, *J. Phys. Chem. A*, 2010, **114**, 6803-6810.
31. S. A. C. McDowell and A. D. Buckingham, *J. Am. Chem. Soc.*, 2005, **127**, 15515 - 15520.
32. W. Zierkiewicz, R. Zaleśny and P. Hobza, *Phys. Chem. Chem. Phys.*, 2013, **15**, 6001-6007.
33. Y. Mao and M. Head-Gordon, *J. Phys. Chem. Lett.*, 2019, **10**, 3899-3905.
34. P. Chopra and S. Chakraborty, *Chem. Phys.*, 2018, **500**, 54-61.
35. X. Chang, Y. Zhang, X. Weng, P. Su, W. Wu and Y. Mo, *J. Phys. Chem. A*, 2016, **120**, 2749-2756.
36. M. Jabłoński, *J. Comput. Chem.*, 2014, **35**, 1739-1747.
37. P.-P. Zhou, W.-Y. Qiu and N.-Z. Jin, *J. Chem. Phys.*, 2012, **137**, 084311.
38. A. K. Chandra and T. Zeegers-Huyskens, *J. Comput. Chem.*, 2012, **33**, 1131-1141.
39. S. J. Grabowski, *J. Phys. Chem. A*, 2011, **115**, 12789-12799.
40. A. Karpfen, *Phys. Chem. Chem. Phys.*, 2011, **13**, 14194-14201.
41. O. Donoso-Tauda, P. Jaque and J. C. Santos, *Phys. Chem. Chem. Phys.*, 2011, **13**, 1552-1559.
42. W. Wang, Y. Zhang and B. Ji, *J. Phys. Chem. A*, 2010, **114**, 7257-7260.
43. A. Mukhopadhyay, P. Pandey and T. Chakraborty, *J. Phys. Chem. A*, 2010, **114**, 5026-5033.
44. A. V. Afonin and A. V. Vashchenko, *J. Mol. Struct. (Theochem)*, 2010, **940**, 56-60.
45. B. Michielsen, W. A. Herrebout and B. J. van der Veken, *ChemPhysChem.*, 2008, **9**, 1693-1701.
46. Y. Yang, W.-J. Zhang and X.-M. Gao, *Chin. J. Chem.*, 2006, **24**, 887-893.
47. A. Y. Li, *J. Chem. Phys.*, 2007, **126**, 154102.
48. J. Joseph and E. D. Jemmis, *J. Am. Chem. Soc.*, 2007, **129**, 4620-4632.

49. W. Zierkiewicz, P. Jurecka and P. Hobza, *ChemPhysChem.*, 2005, **6**, 609-617.
50. K. Hermansson, *J. Phys. Chem. A*, 2002, **106**, 4695-4702.
51. S. Scheiner and T. Kar, *J. Phys. Chem. A*, 2002, **106**, 1784-1789.
52. R. D. Parra and S. J. Grabowski, *Int. J. Mol. Sci.*, 2022, **23**, 11289.
53. S. J. Grabowski, *Chem. Phys. Lett.*, 2014, **605-606**, 131-136.
54. J. E. Del Bene, I. Alkorta and J. Elguero, *Chem. Phys. Lett.*, 2020, **761**, 137916.
55. I. Alkorta, J. Elguero and J. M. Oliva-Enrich, *Materials*, 2020, **13**, 2163.
56. A. S. Mikherdov, R. A. Popov, A. S. Smirnov, A. A. Eliseeva, A. S. Novikov, V. P. Boyarskiy, R. M. Gomila, A. Frontera, V. Y. Kukushkin and N. A. Bokach, *Cryst. Growth Des.*, 2022, **22**, 6079-6087.
57. D. F. Mertsalov, R. M. Gomila, V. P. Zaytsev, M. S. Grigoriev, E. V. Nikitina, F. I. Zubkov and A. Frontera, *Cryst.*, 2021, **11**, 1406.
58. I. Alkorta and A. C. Legon, *ChemPlusChem*, 2021, **86**, 778-784.
59. I. Alkorta, J. Elguero and A. Frontera, *Cryst.*, 2020, **10**, 180.
60. Y. V. Torubaev, A. V. Rozhkov, I. V. Skabitsky, R. M. Gomila, A. Frontera and V. Y. Kukushkin, *Inorganic Chemistry Frontiers*, 2022, **9**, 5635-5644.
61. G. Mahmoudi, I. Garcia-Santos, M. Pittelkow, F. S. Kamounah, E. Zangrando, M. G. Babashkina, A. Frontera and D. A. Safin, *Acta Cryst. B*, 2022, **78**, 685-694.
62. S. J. Grabowski, *Cryst.*, 2022, **12**, 112.
63. S. J. Grabowski, *Struct. Chem.*, 2019, **30**, 1141-1152.
64. V. Kumar, P. Scilabra, P. Politzer, G. Terraneo, A. Daolio, F. Fernandez-Palacio, J. S. Murray and G. Resnati, *Cryst. Growth Des.*, 2021, **21**, 642-652.
65. P. Politzer, J. S. Murray and T. Clark, *Top. Curr. Chem.*, 2015, **358**, 19-42.
66. F. Yao, N. Gong, W. Fang and Z. Men, *Phys. Chem. Chem. Phys.*, 2020, **22**, 5702-5710.
67. U. Adhikari and S. Scheiner, *J. Phys. Chem. A*, 2012, **116**, 3487-3497.
68. D. Kaur, R. Kaur and B. A. Shiekh, *Struct. Chem.*, 2016, **27**, 961-971.
69. M. Michalczyk, W. Zierkiewicz, R. Wysokiński and S. Scheiner, *Molecules*, 2019, **24**, 3329.
70. J. Lu and S. Scheiner, *Molecules*, 2019, **24**, 2822.
71. W. Zierkiewicz, R. Wiczorek, P. Hobza and D. Michalska, *Phys. Chem. Chem. Phys.*, 2011, **13**, 5105-5113.
72. M. J. Frisch, G. W. Trucks, H. B. Schlegel, G. E. Scuseria, M. A. Robb, J. R. Cheeseman, G. Scalmani, V. Barone, G. A. Petersson, H. Nakatsuji, X. Li, M. Caricato, A. V. Marenich, J. Bloino, B. G. Janesko, R. Gomperts, B. Mennucci, H. P. Hratchian, J. V. Ortiz, A. F. Izmaylov, J. L. Sonnenberg, Williams, F. Ding, F. Lipparini, F. Egidi, J. Goings, B. Peng, A. Petrone, T. Henderson, D. Ranasinghe, V. G. Zakrzewski, J. Gao, N. Rega, G. Zheng, W. Liang, M. Hada, M. Ehara, K. Toyota, R. Fukuda, J. Hasegawa, M. Ishida, T. Nakajima, Y. Honda, O. Kitao, H. Nakai, T. Vreven, K. Throssell, J. A. Montgomery Jr., J. E. Peralta, F. Ogliaro, M. J. Bearpark, J. J. Heyd, E. N. Brothers, K. N. Kudin, V. N. Staroverov, T. A. Keith, R. Kobayashi, J. Normand, K. Raghavachari, A. P. Rendell, J. C. Burant, S. S. Iyengar, J. Tomasi, M. Cossi, J. M. Millam, M. Klene, C. Adamo, R. Cammi, J. W. Ochterski, R. L. Martin, K. Morokuma, O. Farkas, J. B. Foresman and D. J. Fox, Gaussian 16 Revision C.01; Gaussian, Inc.: Wallingford, CT, USA, 2016.
73. Y. Zhao and D. G. Truhlar, *Theor. Chem. Acc.*, 2008, **120**, 215-241.
74. K. L. Schuchardt, B. T. Didier, T. Elsethagen, L. Sun, V. Gurumoorthi, J. Chase, J. Li and T. L. Windus, *J. Chem. Infor. Model.*, 2007, **47**, 1045-1052.

75. S. F. Boys and F. Bernardi, *Mol. Phys.*, 1970, **19**, 553-566.
76. ADF2014, SCM, Theoretical Chemistry; Vrije Universiteit: Amsterdam, The Netherlands, 2014.
77. K. Kitaura and K. Morokuma, *Int J Quantum Chem*, 1976, **10**, 325-340.
78. G. te Velde, F. M. Bickelhaupt, E. J. Baerends, C. F. Guerra, S. J. A. Van Gisbergen, J. G. Snijders and T. Ziegler, *J Comput Chem*, 2001, **22**, 931-967.
79. A. E. Reed, F. Weinhold, L. A. Curtiss and D. J. Pochatko, *J. Chem. Phys.*, 1986, **84**, 5687-5705.
80. A. E. Reed and F. Weinhold, *J. Chem. Phys.*, 1983, **78**, 4066-4073.
81. T. Lu and F. Chen, *J. Comput. Chem.*, 2012, **33**, 580-592.
82. S. Alvarez, *Dalton Trans*, 2013, **42**, 8617-8636.
83. B. Nepal and S. Scheiner, *Chem. Phys.*, 2015, **456**, 34-40.
84. S. Scheiner, *J. Phys. Chem. A*, 2021, **125**, 308-316.
85. N. Orangi, K. Eskandari, J. C. R. Thacker and P. L. A. Popelier, *ChemPhysChem.*, 2019, **20**, 1922-1930.
86. D. Hauchecorne, B. J. van der Veken, A. Moiana and W. A. Herrebout, *Chem. Phys.*, 2010, **374**, 30-36.
87. T. A. Bramlett and A. J. Matzger, *Chem. Eur. J.*, 2021, **27**, 15472-15478.
88. Y. Mo, D. Danovich and S. Shaik, *J. Mol. Model.*, 2022, **28**, 274.
89. H. Torii, *Phys. Chem. Chem. Phys.*, 2019, **21**, 17118-17125.
90. E. C. Lambert, A. E. Williams, R. C. Fortenberry and N. I. Hammer, *Phys. Chem. Chem. Phys.*, 2022, **24**, 11713-11720.
91. V. d. P. N. Nziko and S. Scheiner, *Phys. Chem. Chem. Phys.*, 2016, **18**, 3581-3590.
92. J. Lapp and S. Scheiner, *The Journal of Physical Chemistry A*, 2021, **125**, 5069-5077.
93. S. Scheiner and S. Hunter, *ChemPhysChem.*, 2022, **23**, e202200011.
94. B. Nepal and S. Scheiner, *Phys. Chem. Chem. Phys.*, 2016, **18**, 18015-18023.
95. S. Scheiner, *CrystEngComm*, 2019, **21**, 2875-2883.
96. S. Scheiner, *Molecules*, 2017, **22**, 1634.
97. W. Wang and P. Hobza, *J. Phys. Chem. A*, 2008, **112**, 4114-4119.